Frequency-Domain Oversampling for Zero-Padded OFDM in Underwater Acoustic Communications

Zhaohui Wang, *Student Member, IEEE,* Shengli Zhou, *Senior Member, IEEE,*
Georgios B. Giannakis, *Fellow, IEEE,* Christian R. Berger, *Member, IEEE,* and Jie Huang

***Abstract*—Although time-domain oversampling of the received baseband signal is common for single-carrier transmissions, the counterpart of frequency-domain oversampling is rarely used for multicarrier transmissions. This is because frequency-domain oversampling cannot be taken advantage of, when using the commonly used low-complexity receiver that assumes orthogonal subcarriers. In this paper, we explore frequency-domain oversampling to improve the system performance of zero-padded orthogonal frequency division multiplexing transmissions over underwater acoustic channels with large Doppler spread. In these channels intercarrier interference has to be addressed explicitly via frequency-domain equalization, which enables inclusion of additional frequency samples at little increased complexity. We use a signal design that enables separate sparse channel estimation and data detection, reducing equalization complexity. Based on both simulation and experimental results, we observe that the receiver with frequency-domain oversampling outperforms the conventional one considerably, where the gain increases as the Doppler spread increases.**

***Index Terms*—OFDM, zero-padding, intercarrier interference, Doppler spread, frequency-domain oversampling.**

I. Introduction

Recently, zero-padded (ZP) orthogonal frequency division multiplexing (OFDM) has been extensively investigated for high data rate underwater acoustic communications [2]–[4]. Following Doppler shift compensation and an overlap-add operation, fast Fourier transform (FFT) is performed on the received block to obtain frequency-domain samples, that are used for subsequent channel estimation and data detection [2]–[4]. However, overlap-adding incurs information loss: it folds a received block that is a linear convolution of the input and the channel, into a *shorter* block that corresponds to a circular convolution of the input with the channel. This fact has been recognized in [5], and alternative receivers have been developed to improve system performance.

In spite of its known suboptimality, the overlap-add operation is used in most ZP-OFDM receivers. This is because on channels that are linear, time-invariant, or can be approximated as such after proper processing [2], [3], the overlap-add operation preserves the orthogonality among subcarriers, which enables low-complexity equalization and demodulation. This is no longer the case on strongly time-varying channels [4], where intercarrier interference (ICI) impairs subcarrier orthogonality, thus requiring adjacent subcarriers to be jointly demodulated.

To avoid information loss incurred by the overlap-add operation, in this paper, we investigate the use of frequency-domain oversampling, hence a larger size FFT, for ZP-OFDM to improve system performance over underwater acoustic channels with large Doppler spread. The system performance is validated using real data collected from field experiments.

We consider the same ZP-OFDM signal design as in [12], [13] that separates data subcarriers from pilot subcarriers using interspersed null subcarriers. This way, channel estimation and data detection can be carried out separately at the receiver, even in channels with large Doppler spread. We further develop a frequency-domain oversampling receiver, that relies on compressed sensing techniques for sparse channel estimation and minimum mean-square error (MMSE) equalization for data detection. The receiver complexity is only increased marginally by the frequency-domain oversampling: the FFT size increases proportionally and the equalizers process more inputs – *but* the equalizer complexity is dominated by the matrix inversion which scales with the number of data symbols – not the observations. In addition to the rectangular pulse-shaping window, we also consider raised-cosine windows in the signal design to further alleviate the ICI.

We evaluate the performance of the proposed receiver using both simulated and real data collected from the SPACE08 experiment, conducted off the coast of Martha's Vineyard, Massachusetts, October 2008, and the WHOI09 experiment, conducted in the Buzzards Bay, Massachusetts, December 2009. Simulation results demonstrate that frequency-domain oversampling improves the system performance considerably, where the performance gain increases as the channel Doppler spread increases. Experimental results verify the benefits of

This work is supported by the ONR grants N00014-07-1-0805 (YIP), N00014-09-1-0704 (PECASE), and the NSF grant CNS-0721834. It was presented in part at the IEEE/GLOBECOM 2010 Conference, Florida, USA, December 2010 [1].

Associate Editor: U. Mitra.

Z.-H. Wang, and S. Zhou are with the Department of Electrical and Computer Engineering, University of Connecticut, 371 Fairfield Way U-2157, Storrs, CT 06269, USA (email: {zhwang, shengli}@engr.uconn.edu).

G. B. Giannakis is with the Department of Electrical and Computer Engineering, University of Minnesota, 200 Union Street SE, Minneapolis, MN 55455, USA (email: georgios@ece.umn.edu).

C. R. Berger was with the Department of Electrical and Computer Engineering, Carnegie Mellon University, 5000 Forbes Avenue, Pittsburgh, PA 15213, USA. He is now with the Wireless System R&D Group, Marvell Semiconductor, Santa Clara, CA 95054, USA (email: crberger@marvell.com)

J. Huang was with the Department of Electrical and Computer Engineering, University of Connecticut, 371 Fairfield Way U-2157, Storrs, CT 06269, USA. He is now with the Wireless System R&D Group, Marvell Semiconductor, Santa Clara, CA 95054, USA (email: jie.huang.thyme@gmail.com)

Publisher Item Identifier

frequency-domain oversampling in achieving similar performance with fewer phones than the receiver without oversampling. Interestingly, although a raised-cosine pulse-shaping window improves performance relative to a rectangular window, the performance gain is less pronounced when using frequency-domain oversampling.

In contrast to the time-domain oversampling which has been well investigated in single-carrier transmissions [6], only a few studies on its dual, the frequency-domain oversampling in multicarrier transmissions are available in the literature. In [7], the frequency-domain oversampled measurements are used via nonlinear operations to achieve blind carrier-frequency-offset (CFO) recovery for OFDM systems. In [8], frequency-domain oversampling is introduced to capture the structure of multiuser signals for the multiple-access interference (MAI) suppression in an uplink multicarrier (MC)-CDMA system. In [9], three single-user MMSE detectors with frequency-domain oversampling for downlink MC-CDMA system are developed to suppress the MAI. In [10], an adaptive equalization scheme is proposed for OFDM systems based on the oversampled frequency measurements to compensate the CFO effect. In [11], an MMSE equalization approach with frequency-domain oversampling for OFDM is investigated. It shows that the channel frequency diversity can be collected through the frequency-domain oversampling.

At the outset, this paper distinguishes itself from the above works in the following aspects: (i) The receivers in [5], [7]–[11] are based on the narrowband system, while this paper considers a wideband system with large Doppler spreads; (ii) The receivers in those works assume perfect channel knowledge, while this paper deals with both channel estimation and data detection; (iii) The performance results in those works are based on simulations only, where the FFT block sizes are considerably smaller than those used in practical systems.

The contribution of this paper lies in providing concrete evidence to demonstrate the benefit of frequency-domain oversampling in practical systems. This study could motivate further research on frequency-domain oversampling in other scenarios. In addition to multicarrier transmissions, frequency-domain oversampling could also be useful for single-carrier transmissions with frequency-domain equalization, see, e.g., [14].

The rest of the paper is organized as follows. The system model is introduced in Section II. The proposed transmitter and receiver designs are presented in Section III. Numerical simulations are given in Section IV, and experimental results are collected in Sections V and VI. We conclude in Section VII.

Notation: Bold upper-case and lower-case letters denote matrices and column vectors, respectively; $(\cdot)^T$, $(\cdot)^*$, and $(\cdot)^H$ denote transpose, conjugate, and Hermitian transpose, respectively. $\mathbf{I}_N$ stands for an identity matrix with size N.

II. System Model And Motivation

Zero-padded OFDM with rectangular pulse-shaping windows has been used in [2]–[4]. In this paper, we also consider raised-cosine pulse-shaping windows. With T denoting the symbol duration, and β denoting the roll-off factor, the raised-cosine window is [6]

$$g(t) = \begin{cases} 1, & t \in \left[\frac{\beta}{2}T, T\right] \\ \frac{1}{2}\left[1+\cos\left(\frac{\pi}{\beta T}\left(\left|t-\frac{1+\beta}{2}T\right|-\frac{1-\beta}{2}T\right)\right)\right], & t \in \left[0, \frac{\beta}{2}T\right) \cup (T, (1+\beta)T] \\ 0, & \text{otherwise} \end{cases} \quad (1)$$

whose Fourier transform is

$$G(f) = \frac{\sin(\pi f T)}{\pi f T} \cdot \frac{\cos(\pi\beta f T)}{1-4\beta^2 f^2 T^2} e^{-j\pi f(1+\beta)T}. \quad (2)$$

When $\beta = 0$, $g(t)$ in (1) reduces to the rectangular window used in [2]–[4].

With symbol duration T, the subcarrier spacing is $\Delta f = 1/T$, and the subcarriers are located at frequencies

$$f_k = f_c + k/T, \qquad k = -K/2, \ldots, K/2-1, \quad (3)$$

where f_c is the center frequency, and K is the total number of subcarriers, leading to the bandwidth $B = K/T$[1]. Define $\mathcal{S}_A$ and $\mathcal{S}_N$ as the non-overlapping sets of active and null subcarriers respectively, which satisfy $\mathcal{S}_A \cup \mathcal{S}_N = \{-K/2, \ldots, K/2-1\}$. Let $s[k]$ denote the information symbol on the kth subcarrier. The transmitted passband signal is

$$\tilde{x}(t) = 2\text{Re}\left(\sum_{k\in\mathcal{S}_A} s[k] e^{j2\pi f_k t} g(t)\right), \qquad t \in [0, T'], \quad (4)$$

where $T' = (1+\beta)T + T_g$ is the ZP-OFDM block duration accounting for a zero guard time of length T_g; see Fig. 1 for an illustration. The Fourier transform of $\tilde{x}(t)$ for $f > 0$ is

$$\tilde{X}(f) = \sum_{k\in\mathcal{S}_A} s[k] G(f - f_k), \quad (5)$$

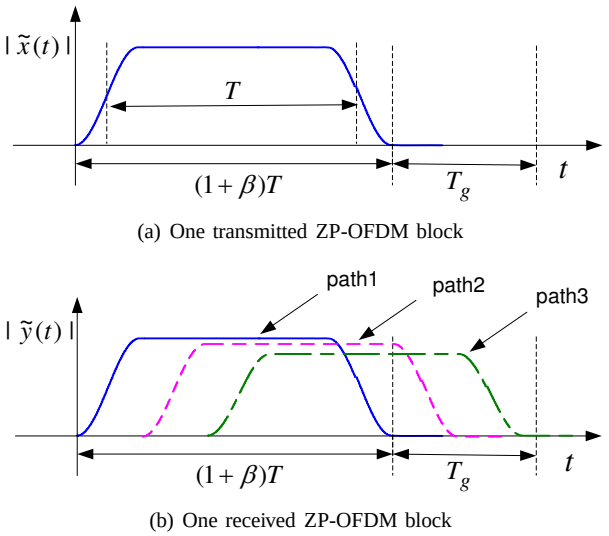

(a) One transmitted ZP-OFDM block

(b) One received ZP-OFDM block

Fig. 1. Illustration of the transmitted and received signals in the time domain.

[1]Although $G(f)$ is not exactly band-limited, the bandwidth of OFDM in practical systems is treated as K/T, by turning off a number of subcarriers on the edges of the signal band.

which occupies the frequency band $[f_c - B/2,\ f_c + B/2]$ with some null subcarriers inserted at the edges of the frequency band.

Assume that the channel consists of N_p discrete paths

$$h(\tau; t) = \sum_{p=1}^{N_p} A_p(t)\delta\left(\tau - \tau_p(t)\right), \tag{6}$$

where $A_p(t)$ and $\tau_p(t)$ are the amplitude and delay of the pth path. Within one OFDM block, we assume that (i) the amplitude does not change $A_p(t) \approx A_p$, and (ii) the path delay can be approximated as

$$\tau_p(t) \approx \tau_p - a_p t,$$

where τ_p is the initial delay and a_p is the Doppler rate of the pth path. The parameter a_p can be expressed as $a_p = v_p/c$, where v_p is the relative speed of the transmitter and the receiver projected on the pth path, and c is the sound speed in water. As such, the received passband signal is

$$\tilde{y}(t) = \sum_{p=1}^{N_p} A_p \tilde{x}((1+a_p)t - \tau_p) + \tilde{n}(t), \tag{7}$$

where $\tilde{n}(t)$ is the additive noise.

As described in [2], [4], the receiver first performs a resampling operation on the received passband signal to remove the dominant Doppler effect, leading to $\tilde{z}(t) = \tilde{y}\left(t/(1+\hat{a})\right)$ where $(1+\hat{a})$ is the resampling factor; The resampling factor $\hat{a}$ can be estimated based on the packet length change through the use of preamble and postamble [15], or by a synchronization algorithm based on a cyclic-prefixed OFDM preamble [16]. Then the baseband signal $z(t)$ is obtained with the passband to baseband downshifting and the lowpass filtering, leading to

$$\begin{aligned} z(t) = &\sum_{p=1}^{N_p} A_p e^{j2\pi f_c(b_p t - \tau_p)} \\ &\times \sum_{k\in\mathcal{S}_A} s[k] e^{j2\pi \frac{m}{k}((1+b_p)t - \tau_p)} g((1+b_p)t - \tau_p), \end{aligned} \tag{8}$$

where b_p represents the residual Doppler rate, with

$$1 + b_p = \frac{1+a_p}{1+\hat{a}}. \tag{9}$$

The baseband signal $z(t)$ is often sampled at the baseband rate $K\Delta f$, and hence the sampling interval is T/K. Since null subcarriers are placed at the edges of the signal band, this sampling rate does not incur any information loss. For each ZP-OFDM block, a total of

$$K' \triangleq (1+\beta)K + (T_g/T)K \tag{10}$$

time-domain samples are obtained, which contain all useful information about the current block.

The receivers in [2], [4] first estimate the mean Doppler shift based on the minimization of the energy spilled to null subcarriers [17], [19]. After compensating the mean Doppler shift (say ϵ Hz) on the baseband sequence, FFT operation is performed after overlap-adding. The FFT output on the kth subcarrier can be expressed as

$$\begin{aligned} z[k] &= Z\left(k/T + \epsilon\right) = \tilde{Z}(f_k + \epsilon) \\ &= \tilde{Y}\left((1+\hat{a})(f_k + \epsilon)\right), \quad k = -K/2, \ldots, K/2 - 1 \end{aligned} \tag{11}$$

where $Z(f)$, $\tilde{Z}(f)$, and $\tilde{Y}(f)$ are the Fourier transforms of $z(t)$, $\tilde{z}(t)$, and $\tilde{y}(t)$, respectively. Channel estimation and symbol detection in [2], [4] are performed based on the K frequency-domain samples $\{z[k]\}_{k=-K/2}^{K/2-1}$.

Clearly, the receivers in [2], [4] do not utilize all the information available per ZP-OFDM block: only K frequently-domain samples are retained while there are $K' > K$ time-domain samples. In this paper, the benefit of frequency-domain oversampling is investigated in the context of underwater acoustic communication systems, and is confirmed using data collected from real experiments.

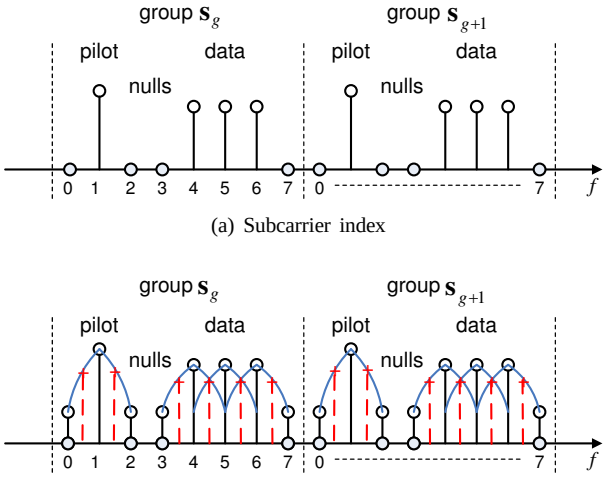

(a) Subcarrier index

(b) solid lines are samples on the subcarriers, while dashed lines are samples mid-way between consecutive subcarriers.

Fig. 2. The subcarrier index and illustration of oversampling with $\alpha = 2$.

III. The Proposed Transceiver Design

We rely on the signal design in [12], [13], where the data subcarriers are separated from the pilot subcarriers by at least two null subcarriers.[2] Specifically, subcarriers are divided into $N_G \triangleq K/8$ groups, with each group containing 8 subcarriers in the following pattern:

$$\begin{bmatrix} 0 & P & 0 & 0 & D & D & D & 0 \end{bmatrix}, \tag{12}$$

where P and D denote a pilot symbol and a data symbol, respectively; see also Fig. 2. For the gth group, the index for the pilot subcarrier is $p_g = (-K/2) + 8g + 1$, and the indexes for the data subcarriers are $i_g - 1, i_g, i_g + 1$, where $i_g = -(K/2) + 8g + 4$. Some subcarrier groups on the edge of the signal band are turned off.

[2] In this paper, we consider only this specific design. The investigation of optimal subcarrier distribution is out of the scope of this paper. Ref. [18] has started to look into this topic with the conventional frequency-domain sampling.

A. Receiver Model

We next present the channel input-output relationship for the signal design in Fig. 2. Using frequency-domain oversampling with an oversampling factor $\alpha \geq 1$, an αK-point FFT operation is performed after padding $\{\alpha K - K'\}$ zeros to the baseband signal after Doppler shift compensation. Therefore, a total of αK frequency-domain samples are obtained. Obviously, when $\alpha = 1$, this operation reduces to the overlap-add receiver. Define

$$\check{f}_{m'} = f_c + \frac{m'}{\alpha T}, \qquad m' = -\alpha K/2, \ldots, \alpha K/2 - 1, \quad (13)$$

where m' and k index of the oversampled measurements and the physical subcarriers, respectively. The measurement $z[m']$ on the frequency $\check{f}_{m'}$ can be related to $z(t)$ as [4]

$$z[m'] = \frac{1}{T}\int_0^{(1+\beta)T+T_g} z(t) e^{-j2\pi\epsilon t} e^{-j2\pi\frac{m'}{\alpha T}t} dt. \quad (14)$$

Substituting (4) and (7) into (14) yields,

$$z[m'] = \sum_{p=1}^{N_p} \left[A'_p e^{-j2\pi(\check{f}_{m'}+\epsilon)\tau'_p} \Big(\sum_{k\in\mathcal{S}_A} \varrho_{m',k}(b_p) s[k] \Big) \right] + \bar{\eta}[m'], \quad (15)$$

where $\bar{\eta}[m']$ is the additive noise and,

$$A'_p = \frac{A_p}{1+b_p}, \qquad \tau'_p = \frac{\tau_p}{1+b_p}, \qquad b_p = \frac{a_p - \hat{a}}{1+\hat{a}}, \quad (16)$$

$$\varrho_{m',k}(b_p) = G\left(\check{f}_{m'} - f_k + \frac{\epsilon - b_p \check{f}_{m'}}{1+b_p} \right). \quad (17)$$

We can rewrite (15) as

$$z[m'] = \sum_{k\in\mathcal{S}_A} \bar{H}_{m',k} s[k] + \bar{\eta}[m'], \quad (18)$$

where $k \in \{-K/2, \ldots, K/2-1\}$ is the subcarrier index, $m' \in \{-\alpha K/2, \ldots, \alpha K/2 - 1\}$ is the index for the FFT outputs, and

$$\bar{H}_{m',k} = \sum_{p=1}^{N_p} A'_p e^{-j2\pi(\check{f}_{m'}+\epsilon)\tau'_p} \varrho_{m',k}(b_p). \quad (19)$$

To separate channel estimation from data detection, we assume that the ICI beyond the direct subcarrier neighbors can be neglected [20]. Specifically, define

$$H_{m',k} = \begin{cases} \bar{H}_{m',k} & |m'/\alpha - k| \leqslant 1 \\ 0 & \text{otherwise} \end{cases}. \quad (20)$$

Eq. (18) can then be rewritten as:

$$z[m'] = \sum_{k\in\mathcal{S}_A} H_{m',k} s[k] + \eta[m']. \quad (21)$$

Clearly, the effective noise is

$$\eta[m'] = \sum_{k\in\mathcal{S}_A} \left(\bar{H}_{m',k} - H_{m',k} \right) s[k] + \bar{\eta}[m']. \quad (22)$$

which consists of the ambient noise and the residual ICI.

B. Sparse Channel Estimation

With the development of compressive sensing techniques, recent publications on the sparse channel estimation tend to be abundant, see, e.g. [21]–[25] and reference therein. However, most of them are limited to narrowband systems, which address multipath channels with different Doppler shifts rather than with different Doppler scales. We next extend the channel estimator from our previous work in [4] to incorporate the frequency-domain oversampling.

Based on (21), the receiver draws the following $2\alpha + 1$ frequency-domain samples for each pilot symbol transmitted as

$$\begin{pmatrix} z[\alpha(p_g-1)] \\ \vdots \\ z[\alpha p_g] \\ \vdots \\ z[\alpha(p_g+1)] \end{pmatrix} = \begin{pmatrix} H_{\alpha(p_g-1),p_g} \\ \vdots \\ H_{\alpha p_g,p_g} \\ \vdots \\ H_{\alpha(p_g+1),p_g} \end{pmatrix} s[p_g] + \begin{pmatrix} \eta[\alpha(p_g-1)] \\ \vdots \\ \eta[\alpha p_g] \\ \vdots \\ \eta[\alpha(p_g+1)] \end{pmatrix}. \quad (23)$$

The channel's frequency response at frequency $\check{f}_{m'}$ can be obtained as

$$\hat{H}_{m',p_g} = z[m']/s[p_g], \qquad m' = \alpha(p_g-1), \ldots, \alpha(p_g+1), \quad (24)$$

in which, corresponding to N_G pilot subcarriers, a total of $N_G(2\alpha+1)$ channel measurements can be collected.

With the limited number of observations, there are much more channel coefficients $\{H_{m',k}\}$ to estimate. Using compressed sensing techniques, the receiver exploits the sparse nature of underwater acoustic channels and jointly estimates the complex gain, Doppler scale, and delay triplets $\{A'_p, b_p, \tau'_p\}_{p=1}^{N_p}$ corresponding to N_p discrete paths. However, this is a *nonlinear* estimation problem, as evidenced by (19). To render the nonlinear estimation problem into a *linear* one, the delay and Doppler scale will be searched over an over-parameterized dictionary, as described next.

Specifically, the sparse channel estimator searches for possible paths on a two dimensional dictionary of (b, τ') of size $N_b \times N_\tau$, with each dimension uniformly discretized as,

$$b \in \{-b_{\max}, -b_{\max} + \Delta b, \ldots, b_{\max}\}, \quad (25)$$

$$\tau' \in \left\{ 0, \frac{T}{\lambda K}, \frac{2T}{\lambda K}, \ldots, T_g \right\}, \quad (26)$$

where Δb and $T/(\lambda K)$ denote the uniform sampling steps along the delay axis and the Doppler rate axis, respectively, with λ an integer to control the time-domain resolution. Hence, there are $N_b N_\tau$ tentative paths to be searched.

The channel measurements of all the groups can be stacked into an $N_G(2\alpha+1) \times 1$ vector,

$$\hat{\mathbf{h}}_P = [\hat{H}_{\alpha(p_0-1),p_0}, \cdots, \hat{H}_{\alpha(p_0+1),p_0}, \cdots, \hat{H}_{\alpha(p_{N_G}-1),p_{N_G}}, \cdots, \hat{H}_{\alpha(p_{N_G}+1),p_{N_G}}]^T, \quad (27)$$

which shall contain the contributions from all possible paths. Let $\xi_{i,j}$ denote the complex amplitude corresponding to the path on the (b_i, τ_j) grid. Based on (27), (19), (20), one can

compactly express $\hat{\mathbf{h}}_P$ as

$$\hat{\mathbf{h}}_P = \sum_{i=1}^{N_b}\sum_{j=1}^{N_\tau} \xi_{i,j}\mathbf{\Lambda}_j\mathbf{\Gamma}_i + \boldsymbol{\eta}_P \tag{28}$$

$$= \underbrace{[\mathbf{\Lambda}_1\mathbf{\Gamma}_1, \ldots, \mathbf{\Lambda}_{N_\tau}\mathbf{\Gamma}_{N_D}]}_{:=\mathbf{A}} \underbrace{\begin{pmatrix} \xi_{1,1} \\ \vdots \\ \xi_{N_D,N_\tau} \end{pmatrix}}_{:=\boldsymbol{\xi}} + \boldsymbol{\eta}_P, \tag{29}$$

with $\boldsymbol{\eta}_P$ denoting the channel measurement noise, and

$$\mathbf{\Lambda}_j = \text{diag}\left(e^{-j2\pi(\check{f}_{m'}+\epsilon)\tau'_j}\right),$$
$$[\mathbf{\Gamma}_i]_{m',l} = \begin{cases} \varrho_{m',l}(b_i) & |m'/\alpha - l| \leqslant 1 \\ 0 & \text{otherwise} \end{cases},$$

where, $\varrho_{m',l}(b_i)$ is defined as in (17), $l \in \{p_g\}_{g=0}^{N_G-1}$ and $m' \in \{\alpha(p_g-1), \alpha(p_g-1)+1, \ldots, \alpha(p_g+1)\}_{g=0}^{N_G-1}$, the sizes of $\mathbf{\Lambda}_j$ and $\mathbf{\Gamma}_i$ are $N_G(2\alpha+1)\times N_G(2\alpha+1)$ and $N_G(2\alpha+1)\times N_G$, respectively.

Noticing that most elements of $\boldsymbol{\xi}$ are zero, the sparse channel parameters are found through the optimization problem,

$$\min_{\boldsymbol{\xi}} \quad \|\hat{\mathbf{h}}_P - \mathbf{A}\boldsymbol{\xi}\|_2 + \zeta|\boldsymbol{\xi}|_1, \tag{30}$$

where the constant ζ controls the sparsity of the solution. In this paper, we use the SpaRSA algorithm from [26] to solve (30).

C. MMSE Channel Equalization

Channel equalization is applied on each group separately. For the gth group with three data symbols $s[i_g-1], s[i_g], s[i_g+1]$, the related channel outputs are

$$\underbrace{\begin{pmatrix} z[\alpha(i_g-2)] \\ \vdots \\ z[\alpha i_g] \\ \vdots \\ z[\alpha(i_g+2)] \end{pmatrix}}_{\triangleq\mathbf{z}_g} = \underbrace{\begin{pmatrix} \eta[\alpha(i_g-2)] \\ \vdots \\ \eta[\alpha i_g] \\ \vdots \\ \eta[\alpha(i_g+2)] \end{pmatrix}}_{\triangleq\boldsymbol{\eta}_g} + \tag{31}$$

$$\underbrace{\begin{pmatrix} H_{\alpha(i_g-2),(i_g-1)} & 0 & 0 \\ \vdots & \vdots & \vdots \\ H_{\alpha i_g,(i_g-1)} & H_{\alpha i_g,i_g} & H_{\alpha i_g,(i_g+1)} \\ \vdots & \vdots & \vdots \\ 0 & 0 & H_{\alpha(i_g+2),(i_g+1)} \end{pmatrix}}_{\triangleq\mathbf{H}_g} \underbrace{\begin{pmatrix} s[i_g-1] \\ s[i_g] \\ s[i_g+1] \end{pmatrix}}_{\triangleq\mathbf{d}_g}.$$

The vector $\mathbf{z}_g$ is of length $4\alpha+1$. With $\alpha = 1$ in the conventional receiver, 5 measurements are used to decode 3 symbols, while an oversampling factor of $\alpha = 2$ leads to 9 available measurements to decode 3 symbols.

Given (22), one can find that the equivalent noise $\boldsymbol{\eta}_g$ consists of both the residual ICI and the ambient noise. The residual ICI is colored. Due to the fact that there are more frequency-domain noise samples than the time-domain noise samples due to oversampling, the ambient noise is colored too. Hence, $\boldsymbol{\eta}_g$ is colored. However, the block-by-block receiver is not able to estimate the covariance of $\boldsymbol{\eta}_g$, as it only focuses on one block, and the covariance of the residual ICI component could change drastically from block to block in fast-varying channels. For simplicity, we assume that $\boldsymbol{\eta}_g$ has zero mean and covariance matrix $N_0\mathbf{I}_{4\alpha+1}$, and obtain the noise variance estimate $\hat{N}_0$ as the average energy on the null subcarriers.[3]

With the approximated noise covariance matrix, the MMSE equalizer's output is

$$\hat{\mathbf{d}}_g^{\text{mmse}} = \left(\mathbf{H}_g^H\mathbf{H}_g + \frac{\hat{N}_0}{E_s}\mathbf{I}_3\right)^{-1}\mathbf{H}_g^H\mathbf{z}_g, \tag{32}$$

where E_s is the symbol energy. At high signal-to-noise ratio (SNR), the MMSE equalizer reduces to the zero-forcing (ZF) equalizer given by

$$\hat{\mathbf{d}}_g^{\text{zf}} = \left(\mathbf{H}_g^H\mathbf{H}_g\right)^{-1}\mathbf{H}_g^H\mathbf{z}_g. \tag{33}$$

Other equalizers such as those based on decision feedback (DFE) [6] or Markov Chain Monte Carlo (MCMC) [28], [29] could also be considered. However, since strong nonbinary LDPC channel coding [30] will be used to evaluate the coded block error rate performance, we focus on linear equalizers in this paper.

When multiple receiving hydrophones are available at the receiver, one can stack the measurement vectors $\{\mathbf{z}_g\}$ of all the hydrophones and the corresponding channel matrices $\{\mathbf{H}_g\}$ into a tall vector and a tall matrix, respectively. The equalization schemes in (32) and (33) can be then applied, which only involve inversion of matrices of size 3×3.

IV. Numerical Simulation

The sparse channel consists of $N_p = 10$ discrete paths, where the inter-arrival time follows an exponential distribution with mean 0.5 ms. The amplitudes are Rayleigh distributed with the average power decreasing exponentially with the delay, where the difference between the beginning and the end of the guard time of 13.1 ms is 6 dB. The Doppler rate a_p of each path is drawn from a zero mean Gaussian distribution with standard deviation $\sigma_v f_c/c$, where σ_v denotes the standard deviation of the platform velocity, and c is the sound speed in water being set to 1500 m/s. Hence, the maximum possible Doppler is about $\sqrt{3}\sigma_v f_c/c$. A total of 2000 Monte Carlo runs are used for simulation. In each run, a channel instantiation is generated according to the channel statistics specified above.

The ZP-OFDM signal parameters are tailored according to the setting of the SPACE08 experiment in Table I, with the only exception of $T_g = 13.1$ ms. The subcarrier allocation in Fig. 2 is adopted. Out of the $N_G = K/8 = 128$ groups, 8 groups on each edge of the signal band are turned off for the band protection, while the pilot subcarriers therein are still used to carry pilot symbols. Hence, there are $|\mathcal{S}_P| = 128$ pilot subcarriers and $|\mathcal{S}_D| = 384$ data subcarriers in total. The data

[3]We have tried to pad $(\alpha K - K')$ noise samples rather than zeros for the αK-point FFT to make the ambient white, however, the decoding performance does not improve, or even slightly degrades due to the extra noise samples.

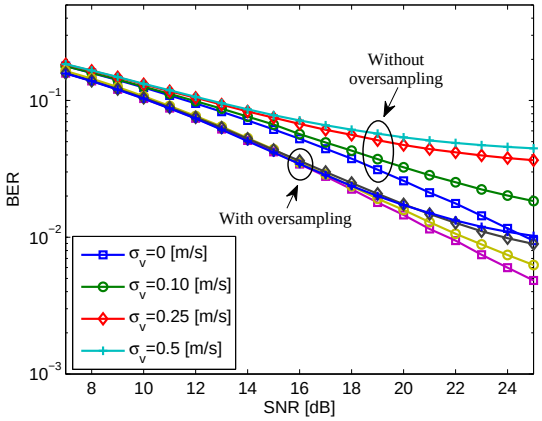

Fig. 3. Uncoded BER bound with full channel knowledge, rectangular window

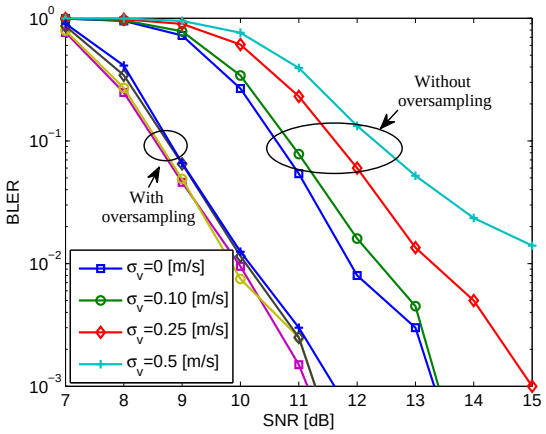

Fig. 4. BLER bound with full channel knowledge, rectangular window

symbols are encoded via a rate-$1/2$ nonbinary LDPC encoder over GF(16) [30] , with each coded symbol mapped to one 16-QAM constellation point, leading to a data rate:

$$R = \frac{1}{2}\frac{|\mathcal{S}_D| \cdot \log_2 16}{(1+\beta)T + T_g} \text{ bits/second.} \quad (34)$$

For raised-cosine windows with $\beta = 0,\ 1/16,\ 1/8$, the overall data rates are $R = 6.5,\ 6.2,\ 5.9$ kb/s, respectively.

The dictionary for the sparse channel estimation are constructed with $\Delta b = \Delta v/c, \Delta v = 0.06$ m/s, $N_D = 15$ and $\lambda = 2$ in (25) and (26), respectively. The MMSE equalizer of Section III-C is adopted for data symbol detection. The block-error-rate (BLER) after channel decoding is used for the performance comparison.

With full channel knowledge, Figs. 3 and 4 demonstrate the uncoded bit-error-rate (BER) and BLER performance bounds with different standard deviations of the Doppler rate. Comparing the performance of conventional and the frequency-oversampling receivers, we observe that the performance of the latter remains almost the same as the Doppler spread increases, while the performance decreases considerably for the receiver without oversampling.

As the channel Doppler spread increases, we can find that the decoding performance of the receiver without frequency oversampling degrades gradually due to severer ICI, whereas

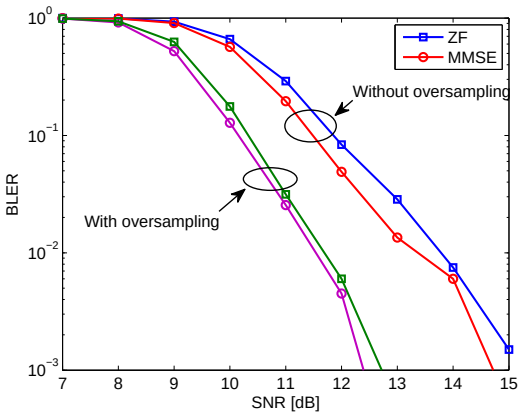

Fig. 5. BLER performance with estimated channels, rectangular window, $\sigma_v = 0.25$ m/s

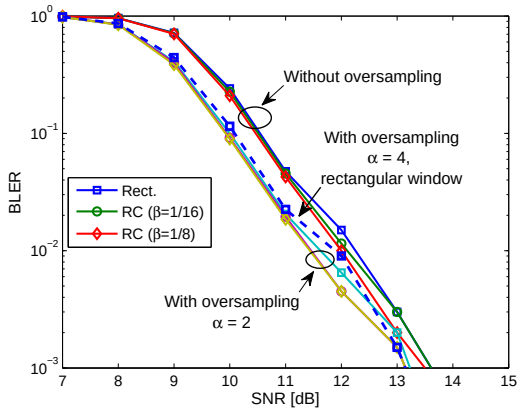

(a) $\sigma_v = 0.10$ m/s

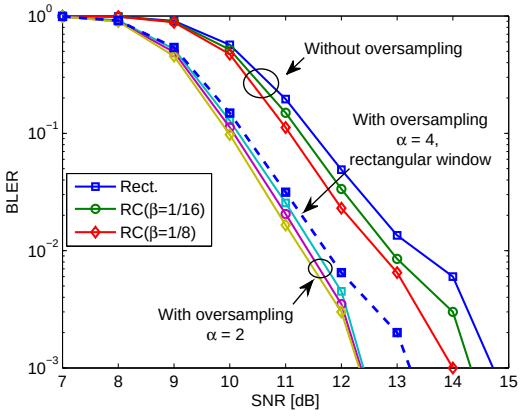

(b) $\sigma_v = 0.25$ m/s

Fig. 6. BLER performance with estimated channels

the performance of the receiver with frequency-domain oversampling does not decrease much, as shown in Fig. 4. Hence, the advantage of frequency-domain oversampling gets pronounced as the Doppler spread increases.

Fig. 5 shows the BLER curves with estimated channel knowledge where both MMSE and zero-forcing (ZF) equalizer are adopted. One can find that the frequency oversampling receiver outperforms the conventional sampling receiver by

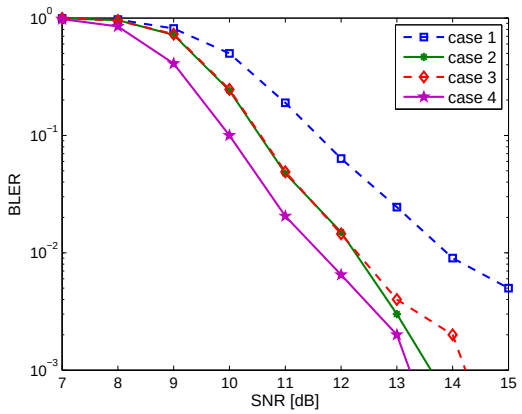

Fig. 7. BLER performance with estimated channels, rectangular window, $\sigma_v = 0.10$ m/s

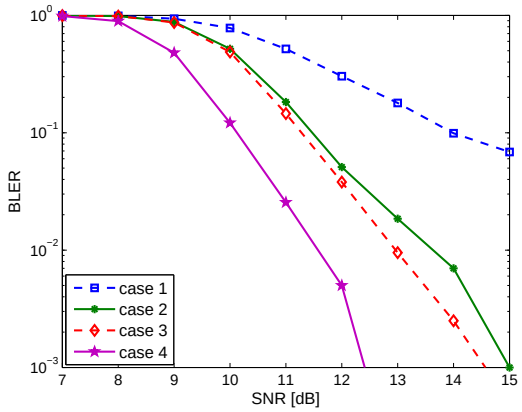

Fig. 8. BLER performance with estimated channels, rectangular window, $\sigma_v = 0.25$ m/s

about 1.5 dB, while the improvement of MMSE equalizer relative to the ZF equalizer is slight.

Figs. 6(a) and 6(b) depict the block-error-rate (BLER) performance of two receivers using different windows and different standard deviations of the Doppler rate. For the conventional sampling receiver, the BLER performance of raised-cosine window is better than that of the rectangular window, and the performance gap improves as the roll-off factor increases. However, for the frequency oversampling receiver, the performance gap between the two types of windows becomes very small. Compared with the windowing operation, the performance gain of the frequency-domain oversampling receiver is more pronounced, especially in the scenario with large velocity deviation.

Moreover, Figs. 6(a) and 6(b) also include the BLER performance of the proposed receiver with an oversampling factor of 4 using the rectangular window. One would expect that employing a larger oversampling factor does not bring obvious performance improvement, as an oversampling factor $\alpha = 2$ has already retained all the information of the time-domain samples. In fact, the performance of the receiver with $\alpha = 4$ is slightly worse than that with $\alpha = 2$, as the approximation accuracy on the covariance matrix of the effective noise in

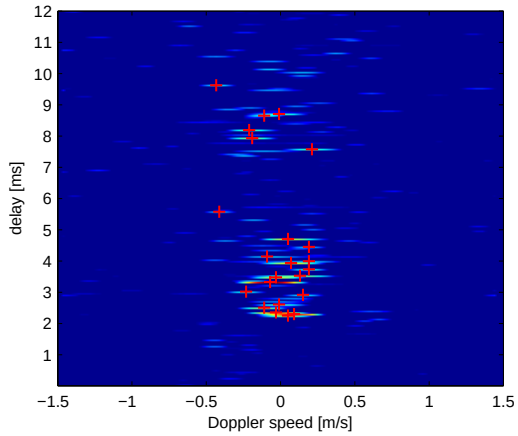

Fig. 9. Sample of sparse channel estimates in the SPACE08 experiment, receiver S3 (1000 m), Julian Data 299.

TABLE I
OFDM PARAMETERS IN SIMULATION AND SPACE08 EXPERIMENT.

f_c	13 kHz
B	9.77 kHz
K	1024
T	104.86 ms
$\Delta f := 1/T$	9.54 Hz
T_g	24.6 ms

(22) decreases with a larger oversampling factor.

To understand how much frequency-oversampling helps on different receiver modules, we plot in Figs. 7 and 8 the BLER performance of receivers of four different cases:

- Case 1): conventional sampling for channel estimation and oversampling for data detection;
- Case 2): conventional sampling for both channel estimation and data detection;
- Case 3): oversampling for channel estimation and conventional sampling for data detection;
- Case 4): oversampling for both channel estimation and data detection.

One can find the receiver performance degrades significantly if frequency-domain oversampling is only applied for data symbol detection (case 1), since the channel information at those additional frequency sampling points is not explicitly available. The performance of the receiver in case 3 is slightly better than that of the receiver in case 2. Hence, data detection with conventional sampling cannot effectively benefit from the improved channel information due to frequency oversampling. Considerable performance improvement is achieved only when frequency-domain oversampling is used for both channel estimation and data detection.

V. SPACE08 EXPERIMENTAL RESULTS

This experiment was held off the coast of Martha's Vineyard, Massachusetts, from Oct. 14 to Nov. 1, 2008. The water depth was about 15 meters. Among all the six receivers, we only consider the data collected by three receivers, labeled as S1, S3, S5, which were 60 m, 200 m, and 1000 m away from the transmitter. Each receiver array consists of twelve

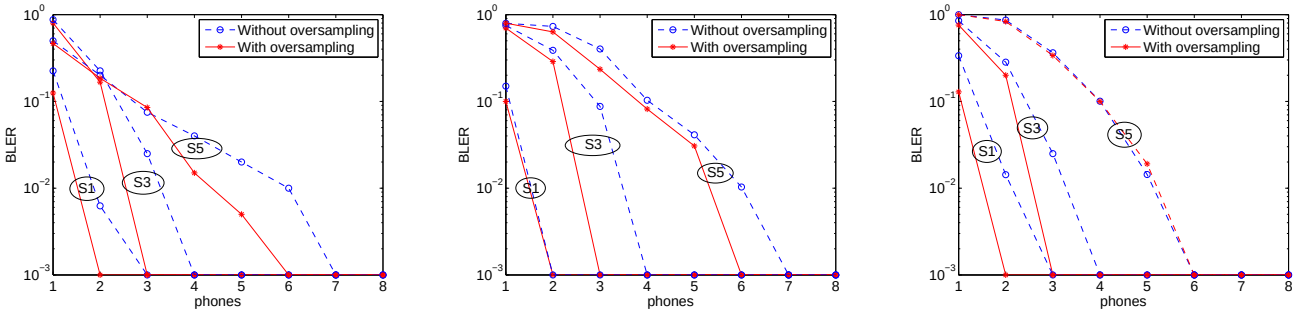

(a) Julian Date 299 (b) Julian Date 300 (c) Julian Date 301

Fig. 10. BLER performance with stationary receivers in the SPACE08 experiment.

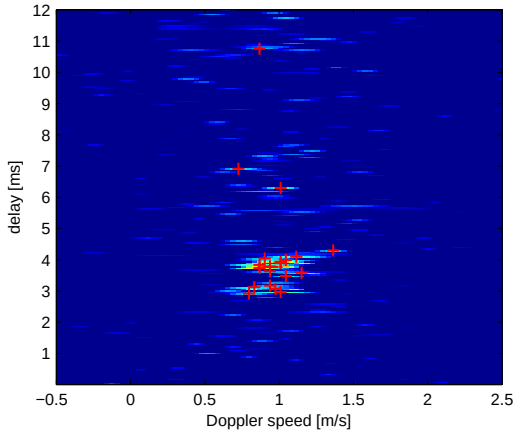

Fig. 11. Sample of sparse channel estimates in the SPACE08 experiment, moving receiver.

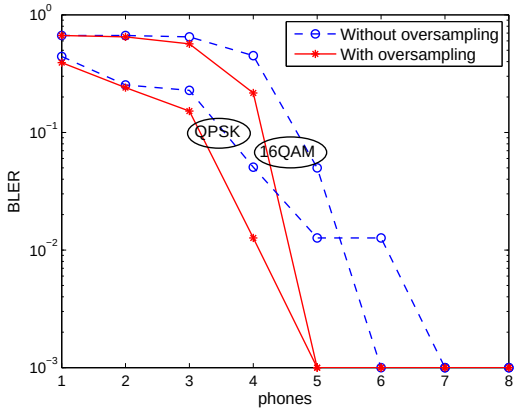

(a) without resampling

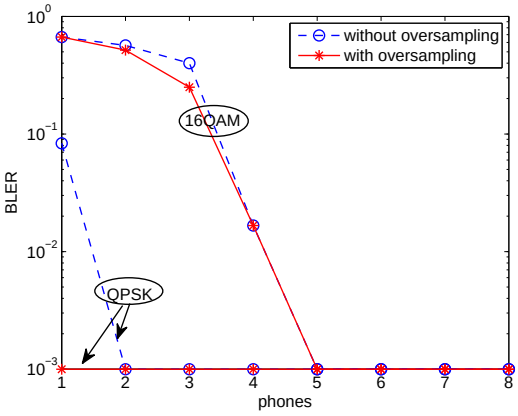

(b) with resampling

Fig. 12. BLER performance with moving receivers.

hydrophones. During the experiment, there are two periods, one around Julian date 297 and the other around Julian date 300 [4], when the wave height and wind speed were larger than those in the rest of days. The later period was more severe. We only consider the data recorded from Julian dates 299-301, the days around the second period. For each day, there are ten recorded files, each consisting of twenty OFDM blocks. Parameter settings of this experiment are summarized in Table I.

A. BLER Performance with Stationary Receivers

Due to the mild Doppler effect, resampling operation is not performed. One example of the estimated paths on the delay-Doppler plane on Julian date 299 is shown in Fig. 9. The average SNR measured in the frequency domain as the ratio of the received power on the pilot subcacarriers to that on the null subcarrers, is mainly distributed from 8 dB to 16 dB. The BLER performance of the received signal on Julian dates 299-301 by combining an increasing number of phones is shown in Fig. 10. Compared with the conventional sampling, frequency-domain oversampling helps to achieve similar performance with less number of phones. Note that multiple factors could affect the experimental decoding results. Similar decoding performance of the receivers with and without frequency-domain oversampling for some settings (e.g., S1 in Fig. 10 (b) and S5 in Fig. 10 (c)) is mainly due to limited experimental data sets, as some data blocks could be challenging enough such that no method is effective. Overall, Fig. 10 clearly shows that more frequency-domain observations lead to better channel estimation and symbol detection performance.

B. BLER Performance with Moving Receivers

With the same transmitter, additional data were collected by an 8-element array, towed by a vehicle moving at the speed of about 1 m/s. Four runs of data were collected, each with twenty

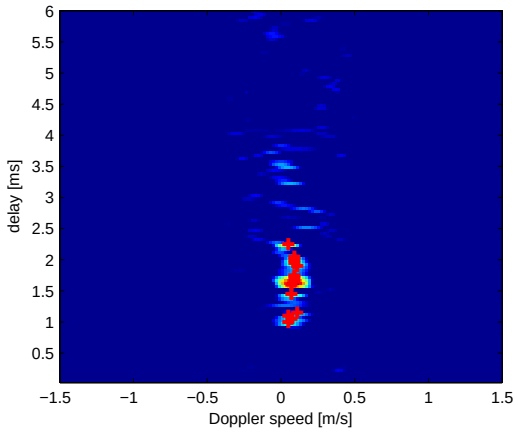

Fig. 13. Sample of sparse channel estimates in the WHOI09 experiment.

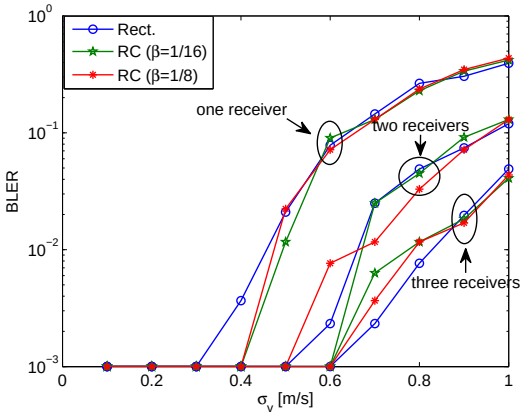

Fig. 14. BLER with conventional sampling, WHOI09 experiment, 16QAM. The received signals are artificially scaled.

OFDM blocks. The estimated resampling factor for each run is $[1.0006,\ 0.9991,\ 0.99913,\ 1.0001]$, which corresponds to a moving speed of $[0.85,\ 1.3,\ 1.35,\ 0.15]$ m/s, respectively. The average SNRs measured in the frequency domain before and after the resampling operation are around 7 dB and 12 dB, respectively. One example of the estimated paths on the delay-Doppler plane is shown in Fig. 11. One can see that the paths are associated with large Doppler rates due to the platform motion. Fig. 12 shows the BLER performance of the conventional sampling method and the frequency oversampling method with and without resampling operation. Due to the motion of the receiving array, the frequency measurements without resampling operation suffer from very large Doppler shifts. Hence, one can see a considerable performance gap between the receiver with resampling operation and that without resampling operation. For the receiver without resampling operation, the performance gain of frequency oversampling is significant due to the large Doppler scaling effect. After removing the main Doppler effect by resampling the received signal, the performance gap between the conventional sampling method and the frequency oversampling method gets decreased, which agrees very well with the simulation results.

VI. WHOI09 Experimental Results

This experiment was carried out in the Buzzards Bay, Massachusetts, from Dec. 07 to Dec. 08, 2009. The water depth was about 15 meters. Two buoy-based receivers were deployed at 1000 meters and 2000 meters away from the transmitter, each with 4 hydrophones. Due to the malfunction of the second hydrophone during the experiment, we only consider the data recorded by the first, third, and fourth phones. There were three transmissions in total, where each transmission consisted of 15 OFDM blocks using the rectangular window, 15 blocks using a raised-cosine window with $\beta = 1/16$, and the other 15 blocks using a raised-cosine window with $\beta = 1/8$. The ZP-OFDM parameters are as follows: $f_c = 31$ kHz, $B = 10$ kHz, $K = 1024$, $T = 102.4$ ms, and $T_g = 24$ ms.

One example of the estimated paths on the delay-Doppler plane is shown in Fig. 13. Due to the calm environment and large SNRs around 30 dB, most received blocks can be decoded with just one phone, hence, the performance difference between different settings is hard to tell. To enlarge the difference, the received signal is decoded without the Doppler shift compensation step [2]. We here only consider the signal received at the buoy 2000 meters away from the transmitter. The number of decoded blocks in error out of the total 45 blocks are shown in Table II, with 16-QAM constellation and rate-1/2 nonbinary LDPC coding [30]. The benefit of frequency-domain oversampling can be seen.

TABLE II
The number of decoded blocks in error out of 45 blocks; Without Doppler shift compensation

	# of Phones	Rect.	RC (1/16)	RC (1/8)
Without oversampling	1	10	11	6
	2	1	0	1
	3	0	0	0
With oversampling	1	0	0	0
	2	0	0	0
	3	0	0	0

To highlight the performance difference between the window types, the received signal is artificially scaled after main Doppler shift compensation. The scaling factor is chosen according to a zero mean Gaussian distribution with standard deviation σ_v/c. With 50 Monte Carlo runs, the average BLER curves over the three transmissions (each consisting of 50×15 blocks) versus different standard deviation of the velocity are plotted. Fig. 14 shows the average BLER performance over three transmissions of the scaled version of the received signal with scaling factor of v/c. Comparing the BLER performance corresponding to different windows, one can find that the performance using the raised-cosine window is similar to that of rectangular window.

VII. Conclusions

In this paper, we presented a zero-padded OFDM transceiver design with rectangular and raised-cosine pulse-shaping windows for underwater acoustic communications. Numerical and experimental results demonstrated that frequency-domain oversampling improves the system performance considerably, and the gain becomes larger as the channel Doppler spread increases.

ACKNOWLEDGEMENT

We would like to thank Dr. J. Preisig and his team for conducting the SPACE08 experiment, and Mr. L. Freitag and his team for conducting the WHOI09 experiment.

REFERENCES

[1] Z.-H. Wang, S. Zhou, G. Giannakis, C. Berger, and J. Huang, "Frequency-domain oversampling for zero-padded OFDM in underwater acoustic communications," in *Proc. of Global Telecommunications Conf.*, Dec. 2010.

[2] B. Li, S. Zhou, M. Stojanovic, L. Freitag, and P. Willett, "Multicarrier communication over underwater acoustic channels with nonuniform Doppler shifts," *IEEE J. Ocean. Eng.*, vol. 33, no. 2, Apr. 2008.

[3] M. Stojanovic, "Low complexity OFDM detector for underwater channels," in *Proc. of MTS/IEEE OCEANS Conf.*, Boston, MA, Sept. 18-21, 2006.

[4] C. R. Berger, S. Zhou, J. Preisig, and P. Willett, "Sparse channel estimation for multicarrier underwater acoustic communication: From subspace methods to compressed sensing," *IEEE Trans. Signal Processing*, vol. 58, no. 3, pp. 1708–1721, Mar. 2010.

[5] B. Muquet, Z. Wang, G. B. Giannakis, M. de Courville, and P. Duhamel, "Cyclic-prefixing or zero-padding for wireless multicarrier transmissions?" *IEEE Trans. Commun.*, vol. 50, no. 12, pp. 2136–2148, Dec. 2002.

[6] J. G. Proakis, *Digital Communications*, 4th ed. New York: McGraw-Hill, 2001.

[7] M. Luise, M. Marselli, and R. Reggiannini, "Low-complexity blind carrier frequency recovery for OFDM signals over frequency-selective radio channels," *IEEE Trans. Commun.*, vol. 50, no. 7, pp. 1182–1188, 2002.

[8] B. Hombs and J. Lehnert, "Multiple-access interference suppression for MC-CDMA by frequency-domain oversampling," *IEEE Trans. Commun.*, vol. 53, no. 4, pp. 677 – 686, Apr. 2005.

[9] Q. Shi, Y. Guan, Y. Gong, and C. Law, "Receiver design for multicarrier CDMA using frequency-domain oversampling," *IEEE Trans. Wireless Commun.*, vol. 8, no. 5, pp. 2236 –2241, Nov. 2009.

[10] Q. Shi and Y. Karasawa, "Adaptive filtering for OFDM systems with frequency-domain oversampling," in *Proc. of Asia-Pacific Conf. on Communications*, Shanghai, China, Oct. 2009, pp. 186–190.

[11] Q. Shi, L. Liu, Y. L. Guan, and Y. Gong, "Fractionally spaced frequency-domain MMSE receiver for OFDM systems," *IEEE Trans. Veh. Technol.*, vol. 59, no. 9, pp. 4400 –4407, Nov. 2010.

[12] S. Mason, C. R. Berger, S. Zhou, K. Ball, L. Freitag, and P. Willett, "An OFDM design for underwater acoustic channels with Doppler spread," in *Proc. of the 2009 DSP & SPE Workshop*, Marco Island, FL, Jan. 2009.

[13] ——, "Receiver comparisons on an OFDM design for Doppler spread channels," in *Proc. of MTS/IEEE OCEANS Conf.*, Bremen, Germany, May 2009.

[14] Y. R. Zheng, C. Xiao, T. C. Yang, and W.-B. Yang, "Frequency-domain channel estimation and equalization for shallow-water acoustic communications," *Elsevier J. of Physical Commun.*, vol. 3, pp. 48–63, Mar. 2010.

[15] B. S. Sharif, J. Neasham, O. R. Hinton, and A. E. Adams, "A computationally efficient Doppler compensation system for underwater acoustic communications," *IEEE J. Ocean. Eng.*, vol. 25, no. 1, pp. 52–61, Jan. 2000.

[16] S. Mason, C. R. Berger, S. Zhou, and P. Willett, "Detection, synchronization, and Doppler scale estimation with multicarrier waveforms in underwater acoustic communication," *IEEE Journal on Selected Areas in Communications*, vol. 26, no. 9, pp. 1638–1649, Dec. 2008.

[17] H. Liu and U. Tureli, "A high efficiency carrier estimator for OFDM communications," *IEEE Commun. Lett.*, vol. 2, pp. 104–106, Apr. 1998.

[18] C. R. Berger, J. P. Gomes, and J. M. F. Moura, "Study of pilot designs for cyclic-prefix OFDM on time-varying and sparse underwater acoustic channels," in *Proc. of MTS/IEEE OCEANS Conf.*, Santander, Spain, Jun. 2011.

[19] X. Ma, C. Tepedelenlioglu, G. B. Giannakis, and S. Barbarossa, "Non-data-aided carrier offset estimations for OFDM with null subcarriers: Identifiability, algorithms, and performance," *IEEE Journal on Selected Areas in Communications*, vol. 19, no. 12, pp. 2504–2515, Dec. 2001.

[20] X. Cai and G. B. Giannakis, "Bounding performance and suppressing intercarrier interference in wireless mobile OFDM," *IEEE Transactions on Communications*, vol. 51, no. 12, pp. 2047–2056, Dec. 2003.

[21] S. F. Cotter and B. D. Rao, "Sparse channel estimation via matching pursuit with application to equalization," *IEEE Trans. Commun.*, vol. 50, no. 3, pp. 374 – 377, Mar. 2002.

[22] C. Carbonelli, S. Vedantam, and U. Mitra, "Sparse channel estimation with zero tap detection," *IEEE Trans. Wireless Commun.*, vol. 6, no. 5, pp. 1743–1763, May 2007.

[23] J. Zhang and A. Papandreou, "Compressive sensing and waveform design for the identification of linear time-varying systems," in *Proc. of Intl. Conf. on Acoustics, Speech and Signal Proc.*, Apr. 2008, pp. 3865 –3868.

[24] R. A. Iltis, "Iterative joint decoding and sparse channel estimation for single-carrier modulation," in *Proc. of Intl. Conf. on Acoustics, Speech and Signal Proc.*, Las Vegas, NV, Apr. 2008, pp. 2689–2692.

[25] G. Tauböck, F. Hlawatsch, D. Eiwen, and H. Rauhut, "Compressive estimation of doubly selective channels in multicarrier systems: Leakage effects and sparsity-enhancing processing," *IEEE J. Select. Topics Signal Proc.*, vol. 4, no. 2, pp. 255–271, Apr. 2010.

[26] S. J. Wright, R. D. Nowak, and M. A. T. Figueiredo, "Sparse reconstruction by separable approximation," *IEEE Trans. Signal Processing*, vol. 57, no. 7, pp. 2479–2493, Jul. 2009.

[27] C. R. Berger, W. Chen, S. Zhou, and J. Huang, "A simple and effective noise whitening method for underwater acoustic orthogonal frequency division multiplexing," *J. Acoust. Soc. Am.*, vol. 127, no. 4, pp. 2358–2367, Apr. 2010.

[28] B. Farhang-Boroujeny, H. Zhu, and Z. Shi, "Markov chain Monte Carlo algorithms for CDMA and MIMO communication systems," *IEEE Trans. Signal Processing*, vol. 54, no. 5, pp. 1896–1909, May. 2006.

[29] R.-R. Chen, R. Peng, B. Farhang-Beroujeny, and A. Ashikhmin, "Approaching MIMO capacity using bitwise Markov chain Monte Carlo detection," *IEEE Trans. Commun.*, vol. 58, no. 2, pp. 423–428, Feb. 2010.

[30] J. Huang, S. Zhou, and P. Willett, "Nonbinary LDPC coding for multicarrier underwater acoustic communication," *IEEE J. Select. Areas Commun.*, vol. 26, no. 9, pp. 1684–1696, Dec. 2008.

Zhaohui Wang (S'10) received the B.S. degree in 2006, from the Beijing University of Chemical Technology (BUCT), and the M.Sc. degree in 2009, from the Institute of Acoustics, Chinese Academy of Sciences (IACAS), Beijing, China, both in electrical engineering. She is currently working toward the Ph.D degree in the Department of Electrical and Computer Engineering at the University of Connecticut (UCONN), Storrs, USA.

Her research interests lie in the areas of communications, signal processing and detection, with recent focus on multicarrier modulation algorithms and signal processing for underwater acoustic communications.

Shengli Zhou (SM'11) received the B.S. degree in 1995 and the M.Sc. degree in 1998, from the University of Science and Technology of China (USTC), Hefei, both in electrical engineering and information science. He received his Ph.D. degree in electrical engineering from the University of Minnesota (UMN), Minneapolis, in 2002.

He has been an assistant professor with the Department of Electrical and Computer Engineering at the University of Connecticut (UCONN), Storrs, 2003-2009, and now is an associate professor. He holds a United Technologies Corporation (UTC) Professorship in Engineering Innovation, 2008-2011. His general research interests lie in the areas of wireless communications and signal processing. His recent focus is on underwater acoustic communications and networking.

Dr. Zhou served as an associate editor for IEEE Transactions on Wireless Communications, Feb. 2005 – Jan. 2007, and IEEE Transactions on Signal Processing, Oct. 2008 – Oct. 2010. He is now an associate editor for IEEE Journal of Oceanic Engineering. He received the 2007 ONR Young Investigator award and the 2007 Presidential Early Career Award for Scientists and Engineers (PECASE).

G. B. Giannakis (Fellow'97) received his Diploma in Electrical Engr. from the Ntl. Tech. Univ. of Athens, Greece, 1981. From 1982 to 1986 he was with the Univ. of Southern California (USC), where he received his MSc. in Electrical Engineering, 1983, MSc. in Mathematics, 1986, and Ph.D. in Electrical Engr., 1986. Since 1999 he has been a professor with the Univ. of Minnesota, where he now holds an ADC Chair in Wireless Telecommunications in the ECE Department, and serves as director of the Digital Technology Center.

His general interests span the areas of communications, networking and statistical signal processing - subjects on which he has published more than 300 journal papers, 500 conference papers, 20 book chapters, two edited books and two research monographs. Current research focuses on compressive sensing, cognitive radios, network coding, cross-layer designs, wireless sensors, social and power grid networks. He is the (co-) inventor of twenty patents issued, and the (co-) recipient of seven paper awards from the IEEE Signal Processing (SP) and Communications Societies, including the G. Marconi Prize Paper Award in Wireless Communications. He also received Technical Achievement Awards from the SP Society (2000), from EURASIP (2005), a Young Faculty Teaching Award, and the G. W. Taylor Award for Distinguished Research from the University of Minnesota. He is a Fellow of EURASIP, and has served the IEEE in a number of posts, including that of a Distinguished Lecturer for the IEEE-SP Society.

Christian R. Berger (S'05-M'09) was born in Heidelberg, Germany in 1979. He received the Dipl.-Ing. degree from the Universität Karlsruhe (TH), now Karlsruhe Institute of Technology (KIT), in Karlsruhe, Germany in 2005; the Ph.D. degree from the University of Connecticut, Storrs, in 2009, both in electrical engineering.

From 2009-2011 he was a Post-Doctoral researcher at Carnegie Mellon University, Pittsburgh, PA. He is now a Staff Systems Engineer in the Wireless R&D Group at Marvell Semiconductor, Santa Clara, CA. His research interests are in the area of signal processing for wireless communication, specifically implementation of multicarrier systems such as OFDM, with focus on synchronization, channel estimation, and implementation complexity.

Dr. Berger has served as reviewer for various technical journals and conferences, as well as on the technical program committee of the Fusion conference and the PIMRC symposium.

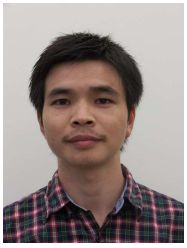

Jie Huang received the B.S. degree in 2001 and the Ph. D. degree in 2006, from the University of Science and Technology of China (USTC), Hefei, China, both in electrical engineering and information science. He was a research assistant professor with the Department of Electrical and Computer Engineering at the University of Connecticut, Storrs. He is now with the Department of Wireless System R&D at the Marvell Semiconductor, Santa Clara.

His general research interests lie in the areas of wireless communications and digital signal processing, specially error control coding theory, network coding theory, digital fountain coding, channel estimation, MIMO equalization, and iterative receiver design.